

**Evidence for a 3.8 MeV state in  ${}^9\text{Be}$** 

R. Smith,<sup>1,\*</sup> C. Wheldon,<sup>1</sup> M. Freer,<sup>1</sup> N. Curtis,<sup>1</sup> Tz. Kokalova,<sup>1</sup> S. Almaraz-Calderon,<sup>2</sup> A. Aprahamian,<sup>2</sup> N. I. Ashwood,<sup>1</sup> M. Barr,<sup>1</sup> B. Bucher,<sup>2</sup> P. Copp,<sup>3</sup> M. Couder,<sup>2</sup> X. Fang,<sup>2</sup> G. Goldring,<sup>4</sup> F. Jung,<sup>2</sup> S. R. Leshner,<sup>3</sup> W. Lu,<sup>2</sup> J. D. Malcolm,<sup>1</sup> A. Roberts,<sup>2</sup> W. P. Tan,<sup>2</sup> and V. A. Ziman<sup>1</sup>

<sup>1</sup>*School of Physics and Astronomy, University of Birmingham Edgbaston, Birmingham B15 2TT, United Kingdom*

<sup>2</sup>*Department of Physics, University of Notre Dame, Notre Dame, Indiana 46556-5670, USA*

<sup>3</sup>*Department of Physics, University of Wisconsin - La Crosse, La Crosse, Wisconsin 54601, USA*

<sup>4</sup>*Department of Particle Physics, Weizmann Institute, 76100 Rehovot, Israel*

(Received 12 May 2016; published 25 July 2016)

The breakup reaction  ${}^9\text{Be}({}^4\text{He}, 3\alpha)n$  was measured using an array of four double-sided silicon strip detectors at beam energies of 22 and 26 MeV. Excited states in  ${}^9\text{Be}$  up to 8 MeV were populated and reconstructed through measurements of the charged reaction products. Evidence is given for a state in  ${}^9\text{Be}$  at  $3.82_{-0.09}^{+0.08}$  MeV with  $\Gamma = 1240_{-90}^{+270}$  keV. This is consistent with two recent measurements of a state with similar properties in the mirror nucleus  ${}^9\text{B}$ . An analysis of the reduced widths ( ${}^8\text{Be}_{\text{g.s.}}$  channel) of this state along with the proposed mirror state has led to a firm limit of  $J \leq 7/2$  and a tentative assignment of  $J^\pi = 1/2^-$  or  $3/2^-$ .

DOI: [10.1103/PhysRevC.94.014320](https://doi.org/10.1103/PhysRevC.94.014320)

**I. INTRODUCTION**

The structures of light nuclei, accessible now through state-of-the-art microscopic *ab initio* calculations, appear to show a wide variety of interesting features including the clustering of nucleons, neutron halos and nuclear molecules. From a theoretical perspective the  $\alpha : n : \alpha$  molecular structure of  ${}^9\text{Be}$  has been successfully described in terms of an exchange neutron being in either  $\sigma$ - or  $\pi$ -type orbitals about two  $\alpha$ -particle cores. These orbitals are analogous to electron orbits in atomic molecules [1]. In agreement with this picture, antisymmetrized molecular dynamics (AMD) and no-core *ab initio* calculations have explicitly illustrated the emergence of  $\alpha$  clustering in  ${}^9\text{Be}$  without assuming this structure *a priori* [2,3].

Despite these exciting advances in nuclear theory  ${}^9\text{Be}$  remains an exceptionally difficult nucleus to study experimentally. Measured states have been tentatively classified into rotational bands with reasonable success [4,5]. However, since the excited states exist as short-lived resonances above the particle decay threshold, evidence of enhanced  $\gamma$  transition rates between band members—a key indicator of collective rotation—is scarce. Therefore, ambiguity remains as to whether the low-lying states in  ${}^9\text{Be}$  are  $\alpha$  clustered or shell-model-like.

Mean-field-type calculations have been shown to satisfactorily reproduce the natural parity experimental spectrum of  ${}^9\text{Be}$  [6], and calculations which utilize an extended Nilsson model space obtain a good fit to the ground state charge form factor for electron scattering [7]. However, it should be noted that in order to correctly describe the properties of the excited  $5/2_1^-$  level at 2.43 MeV (interpreted as a rotational excitation of the ground state in the molecular picture), higher order deformation terms of the Nilsson potential (beyond  $r^2Y_{20}$  prolate shapes) were required. The shape of this deformation was since shown to be consistent with the dumbbell structure of

two  $\alpha$  particles [8]. Furthermore, the particularly low excitation of the first unnatural parity state in  ${}^9\text{Be}$  is difficult to explain in the shell model. This state would involve the promotion of a nucleon into a higher oscillator shell and hence would be expected to have a relatively high excitation energy.

There is significant interest in gaining a complete spectroscopic picture of the low-lying energy regions of the  ${}^9\text{Be}/{}^9\text{B}$  mirror pair. Mirror pairs of nuclei provide information about the charge independence of the nuclear force, and, in certain cases such as this, the Coulomb displacement energy can lead to an understanding of the nuclear structure. Clustered and shell-model configurations possess very different physical sizes; the latter corresponds to a more compact structure. The Coulomb energy is very sensitive to the volume occupied by the valence particle (i.e., its proximity to the other nucleons), which translates into the excitation energy of the states [9]. Therefore, a detailed comparison of the  ${}^9\text{Be}$  and  ${}^9\text{B}$  spectra—replacing a valence neutron with a proton—can provide an insight into the structure of these nuclei.

All excited states in  ${}^9\text{Be}$  are unbound and strongly overlap due to their large widths. Despite decades of extensive experimental efforts, the low-lying spectra of  ${}^9\text{Be}$  (and the  ${}^9\text{B}$  mirror) have not been well elucidated. Epitomizing these experimental challenges, there is a longstanding mystery surrounding the  $1/2^+$  first excited state of  ${}^9\text{B}$  which, despite increased attention in recent years, still remains to be conclusively observed [4,9–11]. Here we report the results of a  ${}^9\text{Be}({}^4\text{He}, 3\alpha)n$  study of the  ${}^9\text{Be}$  spectrum.

**II. EXPERIMENTAL DETAILS**

The present experimental measurements were performed using the FN Tandem Van de Graaff accelerator at the Notre Dame Nuclear Science Laboratory, using a  ${}^4\text{He}^{2+}$  beam at energies of 22 and 26 MeV, incident on a  $1\text{ mg cm}^{-2}$   ${}^9\text{Be}$  target. Excited states in  ${}^9\text{Be}$  were populated through the inelastic scattering channel, resulting in the overall breakup reaction of  ${}^9\text{Be}({}^4\text{He}, 3\alpha)n$ . The experimental setup is detailed

\*r.smith.3@pgr.bham.ac.uk

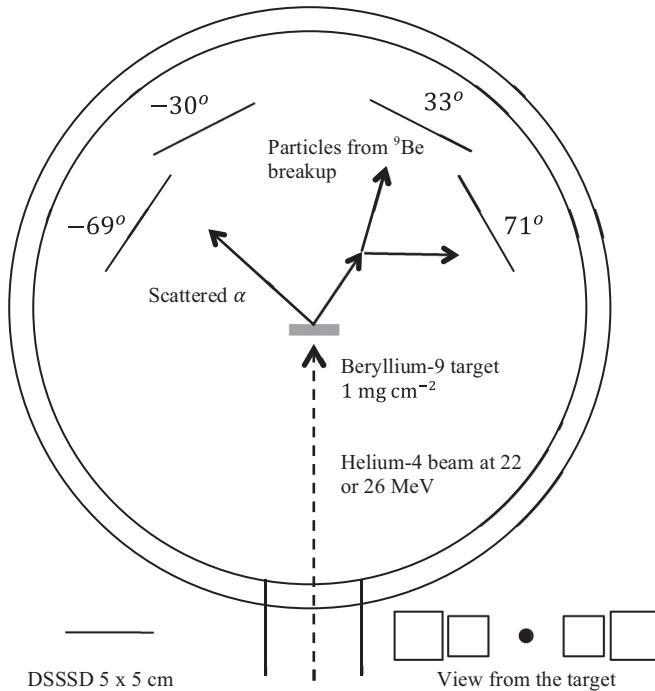


FIG. 1. Schematic drawing of the reaction chamber and detector positions along with an illustration of the inelastic scattering and breakup process.

in Fig. 1. An array of four in-plane 500- $\mu\text{m}$ -thick, Micron W1 (Micron Semiconductor Ltd.) double-sided silicon strip detectors (DSSSDs) was used to detect the charged reaction products. Each DSSSD has a total surface area of  $5 \times 5 \text{ cm}^2$  and was aligned with its plane perpendicular to a line joining the target and detector center. The front and rear faces of each detector were split into 16 horizontal and 16 vertical strips respectively, each with a separate readout, allowing both the energy and the position of a particle to be determined. This allowed the momentum vector of each detected particle to be calculated, assuming each to be an  $\alpha$  particle. Each detector channel was calibrated using  $^{148}\text{Gd}$  and  $^{241}\text{Am}$   $\alpha$  sources and had a typical energy resolution of 60 keV (FWHM). The detectors were placed at distances 6.5, 10.7, 10.9, and 6.8 cm from the target at center angles  $-69^\circ$ ,  $-30^\circ$ ,  $33^\circ$ , and  $71^\circ$  with respect to the beam axis. The positions, angles, and calibrations of the detectors were verified through measuring  $^4\text{He}$  elastic scattering from  $^{197}\text{Au}$  and  $^{12}\text{C}$  targets. In the processing electronics, a multiplicity condition of three coincident hits was demanded for each valid event.

### III. ANALYSIS

Detection of the charged particles resulting from each reaction allowed the excitation of  $^9\text{Be}$  to be calculated on an event-by-event basis. Using the energies and momenta of the detected particles ( $\alpha_i$ ), along with the known energy of the beam, it was possible to reconstruct the properties of the undetected final-state neutron, and gain a complete kinematic description of each event. The momentum of the undetected

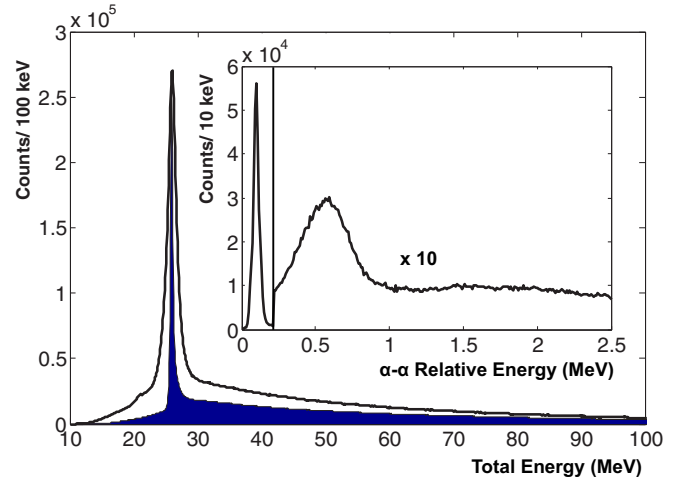


FIG. 2. Sum energy spectra for all four final-state particles, assumed to be  $3\alpha + n$ , corrected for the  $^9\text{Be}(^4\text{He}, 3\alpha)n$  reaction  $Q$  value. The black line and shaded histogram give the spectra before and after target energy loss corrections were applied, respectively. The shaded histogram has been vertically scaled by a factor of 0.5 for plotting. Events within  $2\sigma$  of the corrected peak are identified as  $^9\text{Be}$  breakups. The inset depicts a histogram of the relative energies between pairs of  $\alpha$  particles in the final state. Events residing within the sharp peak at 92 keV correspond to breakup through the  $^8\text{Be}_{g.s.}$  channel.

neutron is given by the equation

$$\mathbf{P}_n = \mathbf{P}_{\text{beam}} - \sum_{i=1}^3 \mathbf{P}_{\alpha_i}. \quad (1)$$

Interactions between the beam and target impurities were rejected by analyzing the *sum energy* of each measured breakup event. Assuming that the beam interacted with a  $^9\text{Be}$  target nucleus, the *sum energy* was calculated by summing the energies of all four final-state particles and subtracting the  $^9\text{Be}(^4\text{He}, 3\alpha)n$  reaction  $Q$  value of  $-1.57 \text{ MeV}$ :

$$E_{\text{sum}} = E_{\text{beam}} = E_n + \sum_{i=1}^3 E_{\alpha_i} - Q. \quad (2)$$

For each event the sum energy was calculated, and this is plotted as the black line histogram in Fig. 2 for the 26 MeV beam data. Due to energy conservation, the sum energy peak is centered near to the beam energy of 26 MeV (FWHM  $\approx 1.9 \text{ MeV}$ ). The small difference and broad peak width are due to the energy loss of the detected particles and the beam in the relatively thick target. These energy losses were corrected before reconstruction of the  $^9\text{Be}$  spectra, and the resulting sum energy spectrum is given by the shaded histogram in Fig. 2. Events within  $2\sigma$  of the corrected peak were accepted for further analysis in order to select the  $^9\text{Be}(^4\text{He}, 3\alpha)n$  reaction of interest. The background to this peak arises from  $^{12}\text{C}$  and  $^{16}\text{O}$  contaminants on the surface of the target. The elastic scattering of the beam was examined in order to determine the composition of the target over each beam run. The relative strengths of each component were determined by normalizing the yield by the Rutherford cross section ( $^9\text{Be}$ : 92%;  $^{12}\text{C}$ : 6%;  $^{16}\text{O}$ : 2%).

Interactions with  ${}^{12}\text{C}$  target impurities were omitted by calculating the sum energy under the assumption of a  ${}^{12}\text{C}({}^4\text{He}, 3\alpha)\alpha$  reaction ( $Q = -7.27$  MeV). If this reaction took place, each of the three measured final-state particles also corresponded to an  $\alpha$  particle. Energy and momentum conservation then allowed the energy of the fourth  $\alpha$  particle to be calculated and a sum energy spectrum to be plotted. Events that resided within this sum energy peak were discarded from further analysis. Due to the complicated five-body final state of the  ${}^{16}\text{O}({}^4\text{He}, 4\alpha)\alpha$  breakup reaction, the  ${}^{16}\text{O}$  contribution was difficult to remove. Gates placed either side of the  ${}^9\text{Be}$  sum energy peak were used to gauge a background profile for the excitation spectra. When further gates were placed later in the analysis, this background was found to be negligible across the majority of the  ${}^9\text{Be}$  spectrum.

In order to calculate the energies of the states populated in  ${}^9\text{Be}$  during the inelastic scattering, it is necessary to identify which of the  $\alpha$  particles in the ambiguous multiparticle final state is the scattered beam particle, and which two arise from the  ${}^9\text{Be}$  breakup. Once this is clear, the resulting excitation in the recoiling  ${}^9\text{Be}$  nucleus can be calculated from the energy and momentum of the scattered beam particle alone. To identify the scattered  ${}^4\text{He}$  in the final state and to provide an additional level of selectivity when examining the possible breakup channels of  ${}^9\text{Be}$ , the relative energies between pairs of  $\alpha$  particles in the final state  $E_{\text{rel}}$  were calculated according to

$$E_{\text{rel}} = \frac{1}{2}\mu v_{\text{rel}}^2, \quad (3)$$

where  $\mu$  is the reduced mass of a pair of  $\alpha$  particles and  $v_{\text{rel}}$  is their relative velocity. Breakup events that proceeded through the  ${}^8\text{Be}_{\text{g.s.}} + n$  channel were selected by gating on the  ${}^8\text{Be}$  ground state lying at  $E_{\text{rel}} = 92$  keV. An  $\alpha$ - $\alpha$  relative energy histogram is shown as the inset of Fig. 2. If the relative energy between two final-state  $\alpha$  particles lay within the narrow  ${}^8\text{Be}_{\text{g.s.}}$  peak, it ensured that the third detected particle corresponds to the scattered beam ( $\alpha_{\text{scatt}}$ ). The background beneath this peak is small (order  $<1\%$ ) so was not considered further in the analysis. The kinetic energy of the recoiling  ${}^9\text{Be}$  nucleus is calculated through momentum conservation:

$$\mathbf{P}_{\text{recoil}} = \mathbf{P}_{\text{beam}} - \mathbf{P}_{\alpha_{\text{scatt}}}, \quad (4)$$

$$E_{\text{recoil}} = \frac{|\mathbf{P}_{\text{recoil}}|^2}{2m_{\alpha}}. \quad (5)$$

Then, using energy conservation, the  ${}^9\text{Be}$  excitation energy is calculated as

$$E_x({}^9\text{Be}) = E_{\text{beam}} - E_{\text{scatt}} - E_{\text{recoil}}. \quad (6)$$

Other breakup channels (namely  ${}^8\text{Be}_{2^+} + n$  and  ${}^5\text{He}_{\text{g.s.}} + {}^4\text{He}$ ) are omitted from further discussion because, in agreement with previous studies, they were found to have strongly overlapping experimental signatures [12,13]. It was therefore not possible to reconstruct clean  ${}^9\text{Be}$  excitation spectra for these decay paths.

Even with the breakup selection criteria in place, there are still a number of contaminant reaction channels that must be accounted for: both  ${}^9\text{Be}({}^4\text{He}, n){}^{12}\text{C}$  and  ${}^9\text{Be}({}^4\text{He}, {}^8\text{Be}_{\text{g.s.}}){}^5\text{He}_{\text{g.s.}}$  reactions are possible and result in the same  $3\alpha + n$  final state. Therefore, in order to further

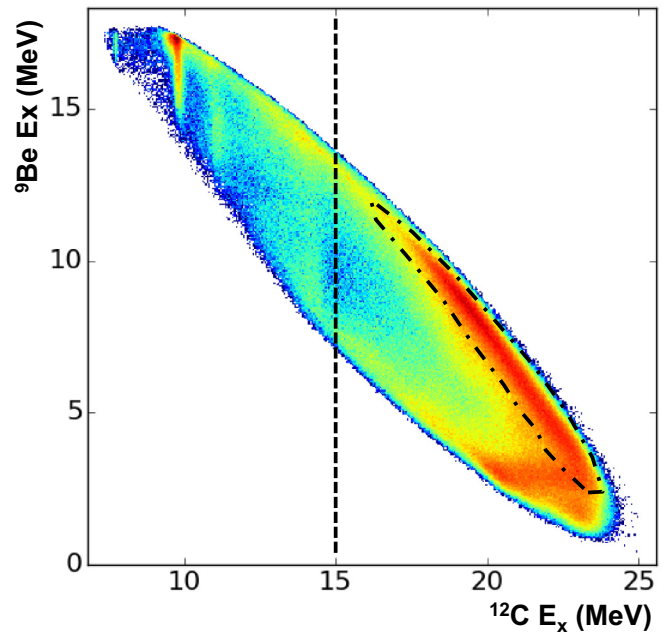


FIG. 3. Dalitz plot for the 26 MeV beam data. Natural parity states associated with  ${}^{12}\text{C}$  breakup appear as vertical bands and  ${}^9\text{Be}$  states form broad, horizontal bands. Neutron transfer events and subsequent breakups of the  ${}^5\text{He}_{\text{g.s.}}$  form the diagonal locus which is surrounded by the dot-dashed line. Only data to the right of the vertical dashed line were considered for further analysis in order to minimize contributions from  ${}^{12}\text{C}$  breakups.

determine the origin of the final state particles, a Dalitz plot was created for each beam-energy run. For this, the excitation in  ${}^9\text{Be}$  [assuming the  ${}^9\text{Be}({}^4\text{He}, 3\alpha)n$  reaction] was plotted against the excitation in  ${}^{12}\text{C}$  [assuming the  ${}^9\text{Be}({}^4\text{He}, n){}^{12}\text{C}$  reaction] on an event-by-event basis. The plot for the 26 MeV beam data is shown in Fig. 3.

Since events involving the  ${}^8\text{Be}_{\text{g.s.}}$  were selected, only states of natural parity in  ${}^{12}\text{C}$  can be seen on the Dalitz plot, appearing as well-defined vertical bands. The low-energy  ${}^{12}\text{C}$  levels (up to the 14 MeV  $4^+$  level) were omitted completely from the analysis by only accepting data that lay to the right of the dashed line in Fig. 3. The intractable broader levels at higher energy in  ${}^{12}\text{C}$  were modeled as a slowly varying background contribution to the  ${}^9\text{Be}$  spectra. Monte Carlo simulations demonstrated that events from the  ${}^9\text{Be}({}^4\text{He}, {}^8\text{Be}_{\text{g.s.}}){}^5\text{He}_{\text{g.s.}}$  reaction occupy the diagonal band and could be cleanly removed by placing software cuts around this region. The resulting  ${}^9\text{Be}$  excitation spectra are acquired by projecting the Dalitz plot onto the vertical axis and are discussed in Sec. IV.

Efficiency profiles for each beam run were evaluated using Monte Carlo simulations of the reaction and the detection geometry. Details of the Monte Carlo code can be found in references [14] and [15]. Isotropic distributions for particle emission were assumed and simulated events were analyzed using the same code as the experimental data to correct for any software gates applied. Although the absolute efficiencies differed if more realistic, anisotropic distributions were used, their relative values for a given breakup channel are mostly insensitive to the nature of the distributions. The efficiency

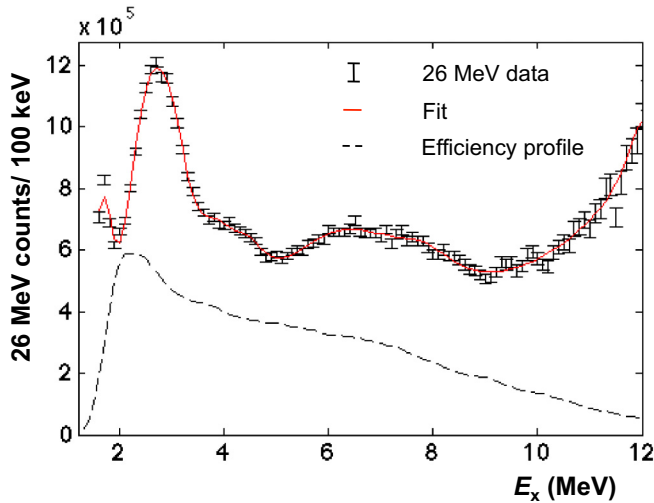


FIG. 4. The scaled Monte Carlo–derived efficiency profile for a 26 MeV beam energy, assuming isotropic particle emission, is given by the dashed line. The experimental data are marked by the points with error bars and the solid (red) line denotes the best fit to the spectrum (see Sec. IV).

profile calculated for the 26 MeV beam data is shown in Fig. 4. The same profile was calculated using various anisotropic angular distributions (forward-focused, backward-focused, exponential). These profiles always maintained the same approximate shape and were found to differ by 3–10 % when normalized. Simulations at 22 MeV beam energy exhibited broadly similar behavior.

#### IV. PEAK FITTING

Initially, the *known* states in  ${}^9\text{Be}$  [4] were fit to the excitation spectra, and the results are shown by the left panel of Fig. 5. The fitted peaks below 3.5 MeV correspond to the Breit-Wigner shape of an isolated resonance convolved with the Gaussian experimental resolution; i.e., Voigt profiles. Monte Carlo simulations showed that high energy states were dominated by a Lorentzian spectral response function. Therefore, the higher excitation states ( $>3.5$  MeV) were fit with a Lorentzian line shape. A thorough investigation of states populated at particularly low excitation requires a detailed multiple-level line-shape analysis due to the proximity of the  ${}^8\text{Be} + n$  threshold [16,17]. However, Monte Carlo simulations demonstrated that the typical experimental resolution was 600–700 keV FWHM—predictably dominant over any threshold dependence of the low energy states. Nonetheless, any small discrepancy in the lowest excitation region is likely attributable to this effect. The simulations demonstrated that the angular resolution of the detectors was the principal contribution to the excitation energy resolution, giving an effect of around 450 keV FWHM. Uncertainties in the beam energy and beam spot size, angular straggling in the target, and the intrinsic detector energy resolution had smaller effects on the overall resolution. The remaining contribution, of around 100 keV FWHM, arises from the imperfect correction for energy losses of the beam and reaction products in the target.

Monte Carlo simulations demonstrated that the excitation energy resolution remained approximately constant over each

of the resonances, justifying the Voigt profile fits. The resolution is notably exceeded by the natural width of many states in the  ${}^9\text{Be}$  spectrum. The centroid and width of each known state were only varied close to the tabulated experimental values [4]. The centroids were typically varied by 100 keV about the tabulated values. The widths, many of which are poorly constrained by previous experiments, were permitted to vary within the experimental uncertainties stated in Ref. [4]. The amplitudes of each peak were free fitting parameters along with the width of the known broad state near 8 MeV (tentative width assignment of  $\approx 1$  MeV). The fits to the two independent experimental (efficiency-corrected) spectra are shown by the left panel of Fig. 5. The fit residuals are plotted as insets to each of these panels. The data were fit using the TRACEY PEAKER V1.0  $\chi^2$  minimization program (MATLAB 2012a) [18].

The fit to the 22 MeV data included a quadratic background and the 26 MeV fit required a slowly varying cubic background. These account for any contributions from  ${}^{12}\text{C}$  breakup not excluded by the Dalitz plot cut in Fig. 3. The different background shapes can be understood by considering the states in  ${}^{12}\text{C}$  which are energetically accessible through the contaminant  ${}^9\text{Be}({}^4\text{He}, n){}^{12}\text{C}$  reaction at each beam energy. The Dalitz plot in Fig. 3 demonstrates that  ${}^{12}\text{C}$  states up to  $\approx 25$  MeV are energetically accessible at the 26 MeV beam energy. States up to  $\approx 21$  MeV were populated at the lower beam energy. In both cases the highest accessible levels in  ${}^{12}\text{C}$  manifest as a background at low  ${}^9\text{Be}$  excitations. Between 20 and 25 MeV there are a higher number of natural parity levels in  ${}^{12}\text{C}$  (a particularly high density of  $1^-$  and  $3^-$  levels) [19]. Since these states are only energetically accessible at the higher beam energy, they will only contribute to the background of the 26 MeV beam energy spectrum. It is also worth noting here that, for the improved fits in the right panels of Fig. 5 (see later), the yield above background is similar across each of the two experimental spectra. This provides further evidence that the two spectra require different background profiles.

The two fits of the known levels are consistent in the low energy region since the populations of each known state are calculated to be approximately the same across each data set. In the region  $<6$  MeV the relative populations generally vary by less than 20% between each fit. This further suggests that the chosen background profiles are reasonable estimations. However, in both cases, the fit is poor in the region of 4 MeV. The discrepancy is more obvious in the 22 MeV plot due to the 26 MeV data set possessing an extra background degree of freedom. Nevertheless, the same systematics manifest in both fits as demonstrated by the fit residuals.

A number of past experimental studies of the  ${}^9\text{Be}$  spectrum, through a variety of different reaction channels, have tentatively noted an increased yield in the 4 MeV region, suggesting that this feature is a real part of the spectrum as opposed to an unaccounted-for experimental effect or background component. A study of high-energy neutron removal from  ${}^{10}\text{Be}$  noted an increased yield around 4 MeV in the  ${}^9\text{Be}$  spectrum albeit with low statistics [20]. Furthermore, inelastic scattering of  ${}^6\text{Li}$  from  ${}^9\text{Be}$  was seen to populate a feature near 4 MeV excitation which could not be reproduced by the known  ${}^9\text{Be}$  levels [12]. Until now, the origin of this feature has not been explored.

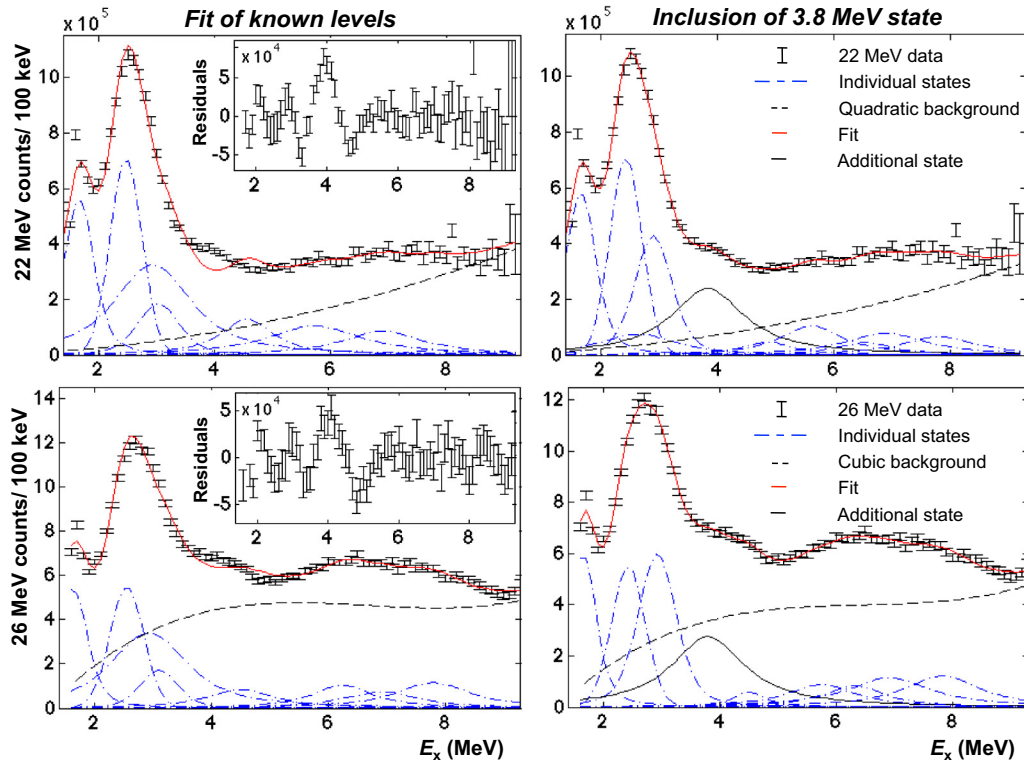


FIG. 5. Peak fits to the  ${}^9\text{Be}$  excitation spectra. Fits of the known levels are shown in the left panels and the fits inclusive of the proposed additional state are shown in the right panels. Plots corresponding to  $E_{\text{beam}} = 22$  and 26 MeV occupy the upper and lower panels respectively. The solid red line on each plot represents the overall fit, individual states are marked by broken dot-dashed lines, and the fitted background profile is marked as a dashed line. In the right panels, the additional level is marked by the solid, black line. The insets of the left panels give the fit residuals, which highlight a discrepancy near 4 MeV excitation.

Further, two recent experiments found evidence for a broad state in the mirror nucleus,  ${}^9\text{B}$ , in this energy region through the  ${}^9\text{Be}({}^3\text{He}, t){}^9\text{B}$  reaction [21,22]. Motivated by the previous published work, an additional state was introduced to the  $\chi^2$  minimization routine and the data were refit. This state was initially chosen to be at 4 MeV with  $\Gamma = 1.5$  MeV, based roughly on the properties of the  ${}^9\text{B}$  state and the behavior of the fit residuals shown in the left panels of Fig. 5. These parameters, along with the amplitude of the level, were allowed to vary freely during the fit. The resulting fits are shown by the right panel of Fig. 5. The newly observed level is highlighted by a solid black line.

Upon inclusion of the additional state, the  $\chi^2$  per degree of freedom fell from 4.81 to 1.17 for the 22 MeV fit and from 3.40 to 0.95 for the 26 MeV fit. Again, roughly consistent populations of states are seen across both data sets. Importantly the centroid and width of the additional level are consistent within uncertainties. For the 22 MeV data set the state is found to be at  $3.83^{+0.09}_{-0.10}$  MeV and  $\Gamma = 1240^{+366}_{-100}$  keV. The 26 MeV fit provides a centroid of  $3.79^{+0.14}_{-0.21}$  MeV and  $\Gamma = 1250^{+390}_{-190}$  keV. If the feature was due to  ${}^{12}\text{C}$  or  ${}^5\text{He}$  breakups (see Fig. 3), it would move significantly in excitation as the total energy of the system (beam energy) is changed. Hence, the consistency in the excitation and width extracted for the state provides good evidence that this is a feature of the  ${}^9\text{Be}$  spectrum.

The quoted  $\chi^2$  values are evaluated in the region  $> 1.8$  MeV due to a particularly poor fit at the lowest energies. This is

expected due to the inability of the Voigt profile to fit the first excited state which lies just above the neutron decay threshold and has been shown to be highly asymmetric [23]. By comparing the left and right panels of Fig. 5 it is clear to see that the fit below 1.8 MeV is the same irrespective of the inclusion of an extra level. This indicates that the poor fit in this region does not reduce the sensitivity of  $\chi^2$  to the new 3.8 MeV level parameters.

The uncertainties quoted correspond to an increase of  $\chi^2$  by one unit when the multidimensional  $\chi^2$  distribution is projected onto the parameter of interest [24]. The  $\chi^2$  dependencies of the energy, width, and amplitude of the additional state, for both fits, are given in Fig. 6. For comparison with the present results, the values of  $E_x$ ,  $\Gamma$ , and  $J^\pi$  available in the most recent compilations are given in Table I. The sensitivity of these many-parameter fits is sometimes poor due to counting statistics and relatively high backgrounds, especially at higher excitations. The deduced centroids and widths of the low-lying excited states are mostly consistent, within uncertainties, with those in the compilation.

## V. DISCUSSION

In order to learn more about the newly measured level in  ${}^9\text{Be}$  it is instructive to compare the excitation spectrum with that of the mirror nucleus,  ${}^9\text{B}$  (Table II). Up to 3 MeV,  $J^\pi$  assignments allow a clear comparison of the experimental spectra and the

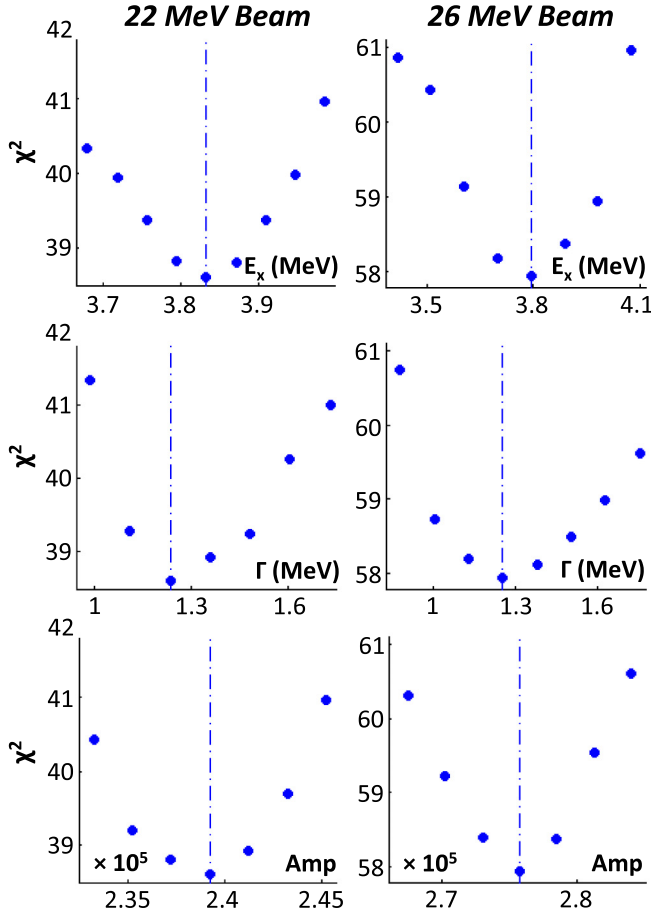


FIG. 6. The sensitivity of the  $\chi^2$  value to the excitation energy (top panels), width (center panels), and amplitude (bottom panels) for the 3.8 MeV state. Fits to the 22 and 26 MeV data are shown in the left and right panels respectively and have  $\chi^2$  per degree of freedom values of 1.17 and 0.95. The horizontal axis of the bottom panel is scaled by a factor of  $10^{-5}$ .

relative excitation energies between these mirror nuclei. Above this energy, the only state in  ${}^9\text{B}$  with a definite  $J^\pi$  assignment is the 7 MeV  $7/2^-$  level. The mirror state in  ${}^9\text{Be}$  at 6.4 MeV is interpreted as the third member of a  $K^\pi = 3/2^-$  rotational band [23,25]. In the intermediate energy region two states exist: a 4.3 MeV level in  ${}^9\text{B}$  which can possibly be identified with the 4.7 MeV level in  ${}^9\text{Be}$ , and the recently measured  ${}^9\text{B}$  level at 3.9 MeV [21,22], which lies at a similar energy to the 3.82 MeV state of the present study.

In the literature, it is seen that the 3.9 MeV  ${}^9\text{B}$  state cross section for  ${}^9\text{Be}({}^3\text{He}, t)$  is characterized by an  $L = 0$  transition, suggesting a negative parity state [21]. The present study of the  ${}^9\text{Be}({}^4\text{He}, 3\alpha)n$  breakup reaction does not easily permit an angular distribution analysis of the data. However, some structural information can be deduced from an analysis of the reduced decay width of the state in question.

The reduced width  $\gamma_i^2$  of a decay channel  $i$  is related to the channel width  $\Gamma_i$  and the penetrability  $P_i$  by  $\gamma_i^2 = \Gamma_i/2P_i$ . The reduced widths are compared with the Wigner single particle limit,  $\gamma_w^2$ , which is the largest theoretically allowed reduced

TABLE I. Comparison of present results with the most recent  ${}^9\text{Be}$  level compilations. The present experimental measurements depict the weighted average of the energies and widths extracted from the 22 and 26 MeV beam-energy fits.

$J^\pi$	Present		Compilation <sup>a</sup>	
	$E_x$ (MeV)	$\Gamma$ (keV)	$E_x$ (MeV)	$\Gamma$ (keV)
$3/2^-$			0	stable
$1/2^+$	$1.65^{+0.03}_{-0.03}$	$260^{+70}_{-50}$	1.684(7)	217(10)
$5/2^-$	$2.43^{+0.02}_{-0.03}$	0.9	2.429(1)	0.78(13)
$1/2^-$	$2.63^{+0.42}_{-0.47}$	$1280^{+90}_{-90}$	2.78(12)	1080(110)
$5/2^+$	$2.92^{+0.05}_{-0.03}$	$270^{+90}_{-100}$	3.049(9)	282(11)
Newly observed state	$3.82^{+0.08}_{-0.09}$	$1240^{+270}_{-90}$		
$(3/2^+)$	$4.65^{+0.31}_{-0.39}$	$610^{+550}_{-520}$	4.704(25)	743(55)
$(3/2^-)$	$5.64^{+0.19}_{-0.18}$	$1080^{+380}_{-370}$	5.59(10)	1330(360)
$7/2^-$	$6.42^{+0.41}_{-0.42}$	$980^{+810}_{-790}$	6.38(6)	1210(230)
$9/2^+$	$6.91^{+0.33}_{-0.37}$	$1430^{+780}_{-540}$	6.76(6)	1330(90)
$(5/2^-)$	$7.82^{+0.33}_{-0.30}$	$1220^{+620}_{-500}$	7.94(8)	$\approx 1000$

<sup>a</sup>Reference [4].

width and corresponds to total ejectile preformation in the decaying nucleus [26]. It has previously been suggested that the widths of states in mirror nuclei can be estimated and compared under the assumption that the ratio of the reduced widths to the Wigner limit ( $\theta^2 = \gamma^2/\gamma_w^2$ ) are equal in the two nuclei (Ref. [27] and references therein). This comparison was used to determine if the measured total widths of the new  ${}^9\text{B}$

TABLE II. Comparison of  ${}^9\text{B}$  and  ${}^9\text{Be}$  levels. A combination of the present measurements and most recent compilations [4]. The horizontal lines highlight the newly measured state in  ${}^9\text{Be}$ .

$J^\pi$ <sup>a</sup>	${}^9\text{B}$		${}^9\text{Be}$	
	$E_x$ (MeV)	$\Gamma$ (keV)	$E_x$ (MeV)	$\Gamma$ (keV)
$3/2^-$	0	0.54(21)	0	stable
$1/2^+$	$\approx 1.6$		1.684(7)	217(10)
$5/2^-$	2.361(5)	81(5)	2.429(1)	0.78(13)
$1/2^-$	2.75(30)	3130(200)	2.78(12)	1080(110)
$5/2^+$	2.788(30)	550(40)	3.049(9)	282(11)
$(\pi = -)^b$	$3.91^{+0.09}_{-0.09}$ <sup>c</sup>	$1520^{+230}_{-210}$ <sup>c</sup>	$3.82^{+0.08}_{-0.09}$	$1240^{+270}_{-90}$
$(3/2^+)$	4.3(2)	1600(200)	4.704(25)	743(55)
$(3/2^-)$			5.59(10)	1330(360)
$7/2^-$	6.97(60)	2000(200)	6.38(6)	1210(230)
$9/2^+$			6.76(6)	1330(90)
$(5/2^-)$			7.94(8)	$\approx 1000$

<sup>a</sup> $J^\pi$  assignments are for  ${}^9\text{Be}$  states. Some of these assignments remain tentative or are absent in  ${}^9\text{B}$  tabulations.

<sup>b</sup>Tentative assignment from Ref. [21].

<sup>c</sup>Weighted average of Refs. [21,22].

TABLE III. Calculation of the ratio of reduced width to Wigner limit ( $\gamma^2/\gamma_w^2$ ) for the  ${}^8\text{Be}_{g.s.}$  channel of the  $5/2^-$  state in  ${}^9\text{B}$  and  ${}^9\text{Be}$ .

$L$	$\theta^2 ({}^9\text{B})$	$\theta^2 ({}^9\text{Be})$
0	$1.7_{-1.0}^{+3.3} \times 10^{-4}$	$9.1_{-3.7}^{+1.1} \times 10^{-6}$
1	$3.0_{-1.8}^{+0.6} \times 10^{-4}$	$2.5_{-1.0}^{+2.9} \times 10^{-5}$
2	$1.3_{-0.7}^{+0.2} \times 10^{-3}$	$3.0_{-1.2}^{+3.5} \times 10^{-4}$
3	$1.5_{-0.9}^{+0.3} \times 10^{-2}$	$1.2_{-0.5}^{+1.4} \times 10^{-2}$
4	$0.36_{-0.21}^{+0.07}$	$0.97_{-0.40}^{+1.14}$

and  ${}^9\text{Be}$  states are consistent with the decay of a state with a particular  $J^\pi$ .

To demonstrate the methodology, the decay of the  $5/2^-$  state in  ${}^9\text{Be}$  and  ${}^9\text{B}$  through the  ${}^8\text{Be}_{g.s.}$  channel is considered. This state has received much attention in both nuclei; although most states in these nuclei decay predominately via a  ${}^8\text{Be}_{g.s.}$  intermediate state, this level has been shown to possess an appreciable  $\alpha$  width in  ${}^9\text{B}$  [9,28]. In  ${}^9\text{Be}$  it decays mainly through the tail of the broad  ${}^8\text{Be}_{2+}$  state [12,13]. It was found to possess similarly small branching ratios (BRs) for decays through the  ${}^8\text{Be}_{g.s.}$ : for the referenced work  $\Gamma_{8\text{Be}_{g.s.}}/\Gamma_{\text{tot}} = 1.8(2)\%$  or  $1.6(8)\%$  for  ${}^9\text{B}$  and  $6(1)\%$  or  $11(2)\%$  for  ${}^9\text{Be}$ .

The CKIN code [29] was used to calculate the penetrabilities and reduced neutron and proton widths using the excitation energies and the widths of the  $5/2^-$  states along with their aforementioned branching ratios. The penetrability can be expressed as a sum of regular and irregular Coulomb wave functions, and CKIN utilizes the Cern Libraries WCLBES code [30,31] to calculate these. The reduced widths were calculated for a number of possible values of the orbital angular momentum of the decay ( $L$ ) and the results are given in Table III. Cases where  $L > 4$  are not shown because the calculated reduced widths exceeded the theoretical Wigner limit. For the case of  $L = 3$  [the expectation for the decay of a  $5/2^-$  state to  ${}^8\text{Be}_{g.s.} (0^+) + n (1/2^+)$ ] the  $\theta^2$  values are consistent within the experimental uncertainties. For  ${}^9\text{B}$   $\theta^2 = 1.46_{-0.85}^{+0.29} \times 10^{-2}$  and for  ${}^9\text{Be}$   $\theta^2 = 1.18_{-0.48}^{+1.39} \times 10^{-2}$ . The other  $L$  values (which are known to be incorrect for this decay channel) differ by around one order of magnitude between the two nuclei and are not consistent within uncertainties. This example demonstrates consistency between the reduced widths for analog states in these nuclei. On a structural level, this rather small reduced width for  $f$ -wave decay along with the measurement of a dominant  $p$ -wave contribution (decays through the  ${}^8\text{Be} 2^+$  first excited state) [13] would appear to indicate that the decay of this state is dominated by the valence space of the lowest-order shell model configuration. Recent no-core configuration interaction calculations agree with this picture [32]. Separating the *ab initio* wave functions into their harmonic oscillator components, using the proton and neutron occupancies, indicated that  $\approx 95\%$  of this state exists in the  $s$  and  $p$  shells. (The exact value depends on the oscillator length, interaction, and degree of convergence, which are discussed in Ref. [25]). Nonetheless, some structural ambiguity remains since microscopic cluster model calculations predict broadly similar decay systematics [33].

TABLE IV. Calculation of the ratio of reduced width to Wigner limit (decays to  ${}^8\text{Be}_{g.s.}$ ) for the 3.9 MeV state in  ${}^9\text{B}$  and the 3.8 MeV state in  ${}^9\text{Be}$  for selected assumed branching ratios.

	$L$	$\theta^2 ({}^9\text{B})$	$\theta^2 ({}^9\text{Be})$
$\Gamma_{8\text{Be}_{g.s.}}/\Gamma_{\text{tot}} = 1$	0	$0.129_{-0.020}^{+0.022}$	$0.122_{-0.011}^{+0.030}$
	1	$0.182_{-0.029}^{+0.032}$	$0.197_{-0.020}^{+0.052}$
	2	$0.467_{-0.081}^{+0.094}$	$0.762_{-0.101}^{+0.244}$
$\Gamma_{8\text{Be}_{g.s.}}/\Gamma_{\text{tot}} = 0.5$	0	$0.065_{-0.010}^{+0.011}$	$0.061_{-0.006}^{+0.015}$
	1	$0.091_{-0.014}^{+0.016}$	$0.099_{-0.010}^{+0.026}$
	2	$0.233_{-0.041}^{+0.047}$	$0.381_{-0.051}^{+0.122}$
$\Gamma_{8\text{Be}_{g.s.}}/\Gamma_{\text{tot}} = 0.1$	0	$0.013_{-0.002}^{+0.002}$	$0.012_{-0.001}^{+0.003}$
	1	$0.018_{-0.003}^{+0.003}$	$0.020_{-0.002}^{+0.005}$
	2	$0.047_{-0.008}^{+0.009}$	$0.076_{-0.010}^{+0.024}$
	3	$0.291_{-0.057}^{+0.069}$	$0.898_{-0.155}^{+0.352}$

The same procedure was applied to the proposed 3.91 and 3.82 MeV mirror states in  ${}^9\text{B}$  and  ${}^9\text{Be}$  respectively. Although the total widths of these states have been measured, the branching ratios are unknown. Therefore, the reduced widths were calculated for the specific cases of  $\Gamma_{8\text{Be}_{g.s.}}/\Gamma_{\text{tot}} = 100\%$ ,  $50\%$ , and  $10\%$  in both nuclei. The absolute values of the calculated  $\gamma_i^2$  depend on the value of this branching ratio but a comparison between the two nuclei depends only on the assumption that they have the same branching ratio. The branching ratios for known states in these nuclei suggest that this assumption is reasonable. Although reliable branching ratio measurements across the two spectra are scarce, key states that have received experimental attention show good correlations. As discussed, the  $5/2^-$  states show a similarly small branching ratio for decays to the  ${}^8\text{Be}_{g.s.}$ . Likewise, the lowest energy  $T = 3/2$  states in these mirror nuclei, which can be selectively populated through  $\beta$  decays, show similar decay systematics under comparison (Table 9.4 of Ref. [4]). Under this condition of comparable branching ratios, the calculated reduced widths are given in Table IV as a function of the orbital angular momentum of the decay. Again, cases where  $\gamma^2 > \gamma_w^2$  are omitted from the table ( $L > 2$  for BR =  $100\%$  and  $50\%$  and  $L > 3$  for BR =  $10\%$ ).

For the cases of  $L = 0$  and  $L = 1$ ,  $\theta^2$  are consistent between the two nuclei within uncertainties. This indicates that if the branching-ratio assumption is correct for these states, then decays through the  ${}^8\text{Be}_{g.s.} + n/p$  channel are  $L = 0$  or  $L = 1$ . This restricts the decaying state in  ${}^9\text{Be}/{}^9\text{B}$  to have  $J = 1/2$  or  $J = 3/2$ . If the tentative negative parity assignment for the state in  ${}^9\text{B}$  [21] is correct then this further restricts the value of  $L$  to 1, corresponding to the decay of a  $1/2^-$  or  $3/2^-$  state. This conclusion strongly relies on the assumption of similar branching ratios for the possible mirror states and therefore the authors encourage the future experimental determination of these quantities as a way to establish the angular momentum and parity of these levels. Furthermore, these branching ratios are required in order to calculate the absolute values of the reduced widths which can be compared with theoretical

calculations. Irrespective of the chosen branching ratios (for  $100\% \geq \Gamma_{8\text{Be}_{g.s.}}/\Gamma_{\text{tot}} \gtrsim 0.5\%$ ) the decay is restricted to  $L < 4$  to ensure that the calculated reduced width does not exceed the Wigner limit. Therefore, there is strong evidence that these states have  $J \leq 7/2$ .

The known spectrum of  ${}^9\text{Be}$  can be well described by three molecular rotational bands ( $K = 3/2^-, 1/2^+$ , and  $1/2^-$  with band heads at 0, 1.68, and 2.78 MeV respectively). Similar band structures are seen in the  ${}^9\text{B}$  mirror. However, a theoretical analysis of two-center molecular states in the beryllium isotopes has also predicted the existence of a  $J = 3/2^+$  molecular band head at an energy higher than those of the other rotational bands [34]. This state corresponds to a  $\pi$ -antibinding configuration of the valence neutron. The reduced widths of the newly measured state suggested an  $L = 0$  or  $L = 1$  decay through the  ${}^8\text{Be}_{g.s.} + n$  channel, consistent with  $J = 3/2$ . (The possibility that the tentative negative parity assignment of the  ${}^9\text{B}$  level is incorrect must also be considered, hence it remains an open possibility that the  $J = 3/2^+$  band head was measured in the present experiment). Once again, the future experimental determination of the branching ratios for this state are encouraged as a possible way to establish its angular momentum and parity.

Under the assumption that the newly measured level in  ${}^9\text{Be}$  and the 3.9 MeV level in  ${}^9\text{B}$  are mirror analogs, something about the structure of the states can be learned from their energies with respect to the  $3/2^-$  ground states. The exchange of a neutron for a proton has a relatively small effect, increasing the excitation energy of the state by  $\approx 110$  keV from  $3.82_{-0.09}^{+0.08}$  MeV (in  ${}^9\text{Be}$ ) to  $3.91_{-0.09}^{+0.08}$  MeV (in  ${}^9\text{B}$ ). Under the assumption of identical wave functions for mirror analog states, the principal way to induce a small energy shift following charge exchange is a diffuse, covalently bound  $\alpha$  structure. This shift is of the same magnitude as the nearby  $5/2^-$

2.43/2.35 MeV  ${}^9\text{Be}/{}^9\text{B}$  analog pair which is known to be strongly  $\alpha$ -clustered. To make a quantitative comparison with the precise magnitude of this shift and the structure described by the underlying wave functions, theoretical input is needed.

## VI. CONCLUSIONS

In summary, a previously unmeasured state in  ${}^9\text{Be}$  was populated in the  ${}^9\text{Be}({}^4\text{He}, 3\alpha)n$  reaction at beam energies of 22 and 26 MeV. The energy and the width of the state were determined by a least-squares fit to the two resulting excitation spectra. The state excitation was found to be  $3.82_{-0.09}^{+0.08}$  MeV with  $\Gamma = 1240_{-90}^{+270}$  keV. An analysis of the reduced widths ( ${}^8\text{Be}_{g.s.}$  channel) of this state along with a proposed mirror analog state in  ${}^9\text{B}$  [21,22] has led to a tentative assignment of  $J^\pi = 1/2^-$  or  $3/2^-$ . A confident assignment of  $J \leq 7/2$  can be made without making assumptions about the absolute branching ratios. The data further allowed the extraction of the width of the 8 MeV state as  $1220_{-500}^{+620}$  keV, building on previous experimental efforts.

## ACKNOWLEDGMENTS

The assistance of the staff at the University of Notre Dame FN tandem facility is gratefully acknowledged. One of the authors (G.G.) would like to thank Prof. Daniel Zajfman and Prof. Yossi Nir of the Weizmann Institute for financial support. R.S. would like to thank M. A. Caprio, P. Maris, and J. P. Vary for illuminating discussions regarding *ab initio* calculations of this nucleus. This work was funded by the United Kingdom Science and Technology Facilities Council (STFC) under Grants No. ST/E500651/1 (C.W.) and No. ST/F011989/1 and by the United States National Science Foundation under Contract No. PHY08-22648.

- 
- [1] W. von Oertzen, *Z. Phys. A* **357**, 355 (1997).  
 [2] Y. Kanada-En'yo and H. Horiuchi, *Prog. Theor. Phys. Suppl.* **142**, 205 (2001).  
 [3] P. Maris and J. P. Vary, *Int. J. Mod. Phys. E* **22**, 1330016 (2013).  
 [4] D. Tilley, J. Kelley, J. Godwin, D. Millener, J. Purcell, C. Sheu, and H. Weller, *Nucl. Phys. A* **745**, 155 (2004).  
 [5] M. Freer, *Rep. Prog. Phys.* **70**, 2149 (2007).  
 [6] C. Adler, T. Corcoran, and C. Mast, *Nucl. Phys.* **88**, 145 (1966).  
 [7] A. Slight, T. Drake, and G. Bishop, *Nucl. Phys. A* **208**, 157 (1973).  
 [8] S. Okabe, Y. Abe, and H. Tanaka, *Prog. Theor. Phys.* **57**, 866 (1977).  
 [9] C. Wheldon, Tz. Kokalova, M. Freer, J. Walshe, R. Hertenberger, H.-F. Wirth, N. I. Ashwood, M. Barr, N. Curtis, Th. Faestermann, R. Lutter, J. D. Malcolm, and D. J. Marín-Lámbarrri, *Phys. Rev. C* **91**, 024308 (2015).  
 [10] R. Sherr and H. T. Fortune, *Phys. Rev. C* **70**, 054312 (2004).  
 [11] H. T. Fortune and R. Sherr, *Nucl. Phys. A* **898**, 78 (2013).  
 [12] T. A. D. Brown, P. Papka, B. R. Fulton, D. L. Watson, S. P. Fox, D. Groombridge, M. Freer, N. M. Clarke, N. I. Ashwood, N. Curtis *et al.*, *Phys. Rev. C* **76**, 054605 (2007).  
 [13] P. Papka, T. A. D. Brown, B. R. Fulton, D. L. Watson, S. P. Fox, D. Groombridge, M. Freer, N. M. Clarke, N. I. Ashwood, N. Curtis, V. Ziman, P. McEwan, S. Ahmed, W. N. Catford, D. Mahboub, C. N. Timis, T. D. Baldwin, and D. C. Weissner, *Phys. Rev. C* **75**, 045803 (2007).  
 [14] N. Curtis, N. M. Clarke, B. R. Fulton, S. J. Hall, M. J. Leddy, A. S. J. Murphy, J. S. Pople, R. P. Ward, W. N. Catford, G. J. Gyapong, S. M. Singer, S. P. G. Chappell, S. P. Fox, C. D. Jones, D. L. Watson, W. D. M. Rae, and P. M. Simmons, *Phys. Rev. C* **51**, 1554 (1995).  
 [15] N. Curtis, A. S. J. Murphy, N. M. Clarke, M. Freer, B. R. Fulton, S. J. Hall, M. J. Leddy, J. S. Pople, G. Tungate, R. P. Ward, W. N. Catford, G. J. Gyapong, S. M. Singer, S. P. G. Chappell, S. P. Fox, C. D. Jones, D. L. Watson, W. D. M. Rae, P. M. Simmons, and P. H. Regan, *Phys. Rev. C* **53**, 1804 (1996).  
 [16] M. A. Tiede, K. W. Kemper, N. R. Fletcher, D. Robson, D. D. Caussyn, S. J. Bennett, J. D. Brown, W. N. Catford, C. D. Jones, D. L. Watson, and W. D. M. Rae, *Phys. Rev. C* **52**, 1315 (1995).  
 [17] A. M. Lane and R. G. Thomas, *Rev. Mod. Phys.* **30**, 257 (1958).  
 [18] R. Smith, TRACEY PEAKER version 1.0 peak fitting code, Matlab File Exchange, 57125, accessed 12-May-2016.  
 [19] F. Ajzenberg-Selove, *Nucl. Phys. A* **506**, 1 (1990).  
 [20] N. I. Ashwood, M. Freer, D. J. Millener, N. A. Orr, F. Carstoiu, S. Ahmed, J. C. Angélique, V. Bouchat, W. N. Catford, N. M. Clarke *et al.*, *Phys. Rev. C* **72**, 024314 (2005).

- [21] H. Akimune, M. Fujimura, M. Fujiwara, K. Hara, T. Ishikawa, T. Kawabata, H. Utsunomiya, T. Yamagata, K. Yamasaki, and M. Yosoi, *Phys. Rev. C* **64**, 041305 (2001).
- [22] C. Scholl, Y. Fujita, T. Adachi, P. von Brentano, H. Fujita, M. Górska, H. Hashimoto, K. Hatanaka, H. Matsubara, K. Nakanishi, T. Ohta, Y. Sakemi, Y. Shimbara, Y. Shimizu, Y. Tameshige, A. Tamii, M. Yosoi, and R. G. T. Zegers, *Phys. Rev. C* **84**, 014308 (2011).
- [23] A. S. Demyanova, A. A. Ogloblin, A. N. Danilov, S. V. Dmitriev, S. A. Goncharov, N. Burtebaev, J. Burtebaeva, N. Saduev, T. L. Belyaeva, H. Suzuki, A. Ozawa, Y. Abe, S. Fukuoka, Y. Ishibashi, S. Ito, T. Komatsubara, T. Moriguchi, D. Nagae, R. Nishikiori, T. Niwa, K. Okumura, H. Ooishi, K. Yokoyama, and S. Kubono, *EPJ Web Conf.* **66**, 02026 (2014).
- [24] W. H. Dress, S. A. Tenkolsky, W. T. Vetterling, and B. P. Flannery, *Numerical Recipes in C. The Art of Scientific Computing* (Cambridge University Press, Cambridge, 1992), Chap. 15, pp. 693–695.
- [25] M. A. Caprio, P. Maris, J. P. Vary, and R. Smith, *Int. J. Mod. Phys. E* **24**, 1541002 (2015).
- [26] T. Teichmann and E. P. Wigner, *Phys. Rev.* **87**, 123 (1952).
- [27] H. T. Fortune and R. Sherr, *Phys. Rev. C* **73**, 024302 (2006).
- [28] E. Gete, L. Buchmann, R. E. Azuma, D. Anthony, N. Bateman, J. C. Chow, J. M. D’Auria, M. Dombisky, U. Giesen, C. Iliadis, K. P. Jackson, J. D. King, D. F. Measday, and A. C. Morton, *Phys. Rev. C* **61**, 064310 (2000).
- [29] C. Wheldon, CKIN 2-body kinematics code, [http://www.np.ph.bham.ac.uk/research\\_resources/programs/](http://www.np.ph.bham.ac.uk/research_resources/programs/), accessed 24-Sep-2014.
- [30] I. McLaren, Wclbes.f subroutine, [http://cernlib.sourcearchive.com/documentation/2006.dfgs.2/wclbes\\_8F\\_source.html](http://cernlib.sourcearchive.com/documentation/2006.dfgs.2/wclbes_8F_source.html), accessed 08-Mar-2016.
- [31] I. Thompson and A. Barnett, *Comput. Phys. Commun.* **36**, 363 (1985).
- [32] M. A. Caprio, P. Maris, and J. P. Vary (private communication).
- [33] P. Descouvemont, *Eur. Phys. J. A* **12**, 413 (2001).
- [34] W. von Oertzen, *Z. Phys. A* **354**, 37 (1996).